Annals of Nuclear Energy 91 (2016) 79–91

Contents lists available at ScienceDirect

Annals of Nuclear Energy

journal homepage: www.elsevier.com/locate/anucene

Validation of the Serpent 2-DYNSUB code sequence using the Special Power Excursion Reactor Test III (SPERT III)

Miriam Knebel [a,*], Luigi Mercatali [a], Victor Sanchez [a], Robert Stieglitz [a], Rafael Macian-Juan [b]

[a] Karlsruhe Institute of Technology, Institute of Neutron Physics and Reactor Technology, Hermann-von-Helmholtz-Platz 1, 76344 Eggenstein-Leopoldshafen, Germany
[b] Technical University of Munich, Department of Nuclear Engineering, Boltzmannstrasse 15, 85748 Garching, Germany

ARTICLE INFO

Article history:
Received 4 October 2015
Received in revised form 6 January 2016
Accepted 7 January 2016
Available online 21 January 2016

Keywords:
Serpent 2/SUBCHANFLOW
DYNSUB
Rod ejection accident
SPERT
Validation

ABSTRACT

The Special Power Excursion Reactor Test III (SPERT III) is studied using the Serpent 2-DYNSUB code sequence in order to validate it for modeling reactivity insertion accidents (RIA) in PWRs. The SPERT III E-core was a thermal research reactor constructed to analyze reactor dynamics. Its configuration resembles a commercial PWR on terms of fuel type, choice of moderator, coolant flow and system pressure. The initial conditions of the rod ejection accident experiments (REA) performed cover cold startup, hot startup, hot standby and operating power scenarios. Eight of these experiments were analyzed in detail. Firstly, multi-dimensional nodal diffusion cross section tables were created for the three-dimensional reactor simulator DYNSUB employing the Monte Carlo neutron transport code Serpent 2. In a second step, DYNSUB stationary simulations were compared to Monte Carlo reference three-dimensional full scale solutions obtained with Serpent 2 (cold startup conditions) and Serpent 2/SUBCHANFLOW (operating power conditions) with a good agreement being observed. The latter tool is an internal coupling of Serpent 2 and the sub-channel thermal-hydraulics code SUBCHANFLOW. Finally, DYNSUB was utilized to study the eight selected transient experiments. Results were found to match measurements well. As the selected experiments cover much of the possible transient (delayed super-critical, prompt super-critical and super-prompt critical excursion) and initial conditions (cold and hot as well as zero, little and full power reactor states) one expects in commercial PWRs, the obtained results give confidence that the Serpent 2-DYNSUB tool chain is suitable to model REAs and other RIAs in PWRs.

1. Introduction

DYNSUB is a reactor simulator being developed at the Karlsruhe Institute of Technology (KIT) (Gomez-Torres et al., 2012a,b). After verifying the code's predictions using well-known international code-to-code benchmarks such as the OECD/NEA and U.S. NRC PWR MOX/UO_2 core transient benchmark (Daeubler et al., 2015b), validation is the next significant phase in its development process. SPERT III (Dugone, 1965; McCardell et al., 1969) provides the unique opportunity to validate DYNSUB using well-documented rod ejection accident (REA) experiments. Of interest for DYNSUB is the SPERT III E-core experiment series that was already used to validate the best-estimate tools TRITON/TRACE/PARCS (Wang et al., 2013), ANCK (Aoki et al., 2009), GALAXY/COSMO-K (Yamaji et al., 2014) and CASMO5/Simalute-3K (Grandi, 2014; Grandi and Moberg, 2012) for PWR applications.

In order to be able to study the SPERT III E-core experiments with DYNSUB, multi-dimensional few-group homogenized cross section tables have to be produced. Using continuous energy (CE) Monte Carlo neutron transport for obtaining few-group homogenized constants for deterministic reactor simulators like DYNSUB has become a popular research topic as reactor simulators and computational capacities evolve. One of the first Monte Carlo codes conceived as a lattice code was Serpent. A study recently found that generating complete multi-dimensional cross section tables with CE Monte Carlo lattice codes has become feasible (Leppänen and Mattila, 2014). The methods to produce few-group homogenized cross sections with Serpent 2 (SSS2) are actively developed by numerous groups, solution verification is ongoing and first efforts to validate the tool have begun (Leppänen et al., 2014a, 2015).

Monte Carlo lattice codes unlike their deterministic counterparts can handle complicated reactor geometries utilizing the best available knowledge on neutron interactions and introduce no major approximations. As a consequence, they are the method of choice to model novel reactor concepts. Introducing Serpent 2 as

* Corresponding author.
E-mail address: miriam.daeubler@gmail.com (M. Knebel).

http://dx.doi.org/10.1016/j.anucene.2016.01.005
0306-4549/

lattice code for DYNSUB is the first step towards extending the range of applicability of DYNSUB from classical light water reactors (LWR) to new reactor designs in the future. Since SSS2's transport simulation is inherently three-dimensional, it has the benefit of being able to produce 3D reference solutions. The majority of deterministic lattice codes, however, are limited to two dimensions. Thanks to the development of coupled Monte Carlo neutron transport thermal-hydraulics code system Serpent 2/SUBCHANFLOW (SSS2/SCF) at KIT (Daeubler et al., 2015a), the unique possibility of producing three-dimensional hot full power (HFP) reference solutions with a lattice code arises.

By studying the SPERT III E-core experiment series, a contribution to the development of cross section generation methodologies for Serpent 2 can be made. All existing verification and validation efforts on creating few-group homogenized cross sections with SSS2 so far were done for hot zero power (HZP) operating conditions and only for static calculations (Leppänen et al., 2014a, 2015). By modeling the SPERT reactivity-initiated accident (RIA) tests with DYNSUB and producing static reference solutions with thermal-hydraulic feedback using SSS2/SCF, for the first time multi-dimensional cross section tables generated with Serpent 2 are assessed under non-zero power and transient conditions.

In this paper, first an overview of the SPERT III E-core experiment series is given. Thereafter, a Serpent 2 and a SSS2/SCF steady-state numerical reference model for both cold startup, i.e. cold zero power, and operating power, i.e. hot full power, conditions are developed. A hot zero power reactor configuration is not considered in this paper since no new insights on the Serpent 2-DYNSUB code sequence can be gained by studying more than one zero power state.

Results obtained with Monte Carlo tools are then used to foster developing and evaluating SSS2 cross section models and a DYNSUB description of the SPERT III E-core. The final DYNSUB model is then employed to study selected experimental transients starting from cold startup, hot standby and operating power conditions.

2. Simulation codes used

2.1. Serpent 2

Serpent 2 (Leppänen, 2013b) is a 3D CE Monte Carlo neutron transport code. It uses a universe-based combinatorial solid geometry (CSG) model as most other Monte Carlo tools do. Neutrons are tracked in the geometry using a combination of surface tracking (ST) and Woodcock delta-tracking (DT). ST is used as a fallback in case the efficiency of DT is too low (Leppänen, 2013a).

Serpent's CE cross sections are given in ACE format. The physics of all interactions are based on classical collision kinematics, ENDF reaction laws and probability table sampling in the unresolved resonance region. All CE cross sections are reconstructed on a unionized energy grid (Leppänen, 2009). Furthermore, a built-in Doppler-broadening pre-processor routine allows for the conversion of any ACE format cross sections to a higher temperature.

A new feature that has been recently introduced into Serpent 2 is a multi-physics interface (Leppänen et al., 2012). The interface may be utilized to exchange data with thermal-hydraulics and fuel performance codes. At KIT, this multi-physics interface has been used as basis to integrate the inhouse sub-channel thermal-hydraulics code SUBCHANFLOW (SCF) into Serpent 2 (Daeubler et al., 2015a).

Serpent 2's predecessor was conceived as a Monte Carlo lattice physics code with the main purpose of generating few-group homogenized constants for deterministic reactor simulators. As a consequence, Serpent 2 is capable of automatically calculating cross section sets for low-order deterministic transport simulations in any of its geometry universes, such as few-group reaction cross sections, scattering matrices and cross sections up to Legendre order 7, diffusion coefficients, assembly discontinuity factors and pin power form factors for pin power reconstruction techniques. The computed cross section sets may be corrected for leakages using a deterministic solution of the multi-group B1 equations (Fridman and Leppänen, 2011). Furthermore, Serpent 2 evaluates effective delayed neutron fractions and point kinetics parameters in each transport simulation.

Serpent 2 has a built-in depletion solver (Leppänen, 2013b). Thus, the evolution of nuclide compositions in fuel being irradiated can be tracked and few-group homogenized cross sections can be generated for entire life cycles of fuel assemblies. For burn-up calculations during which few-group cross sections for use in deterministic reactor simulators are generated, Serpent 2 has a branch capability (Leppänen, 2014). It can change the density and temperature of any material as well as replace entire materials or parts of the overall geometry, i.e. bodies as well as filling materials. Consequently, Serpent 2 can produce complete multi-dimensional cross section tables for deterministic reactor simulators like DYNSUB in a single run.

2.2. Serpent 2/SUBCHANFLOW

An internal coupling between the Monte Carlo code Serpent 2 and the sub-channel code SUBCHANFLOW has been developed at KIT (Daeubler et al., 2015a). In an internal coupling, the thermal-hydraulics tool is integrated into the Monte Carlo neutron transport tool as a module. More importantly, the thermal-hydraulic state point information is separated from the geometry description in the Monte Carlo code allowing for treating arbitrary problem sizes as opposed to externally coupled tools. In an external coupling, Monte Carlo neutron transport tool and the thermal-hydraulics code communicate via in- and output files read/write operations. External couplings generally employ driver scripts or wrapper codes. Such an approach is simple, as it does not require any adaption of the source of any involved tool. However, to be able to handle thermal-hydraulic state point fields, the Monte Carlo geometry in external couplings needs to be subdivided into a multitude of cells each corresponding to one set of TH information. This process is not only error prone but also limits the application of the coupled code to small, academic problems.

This coupling is based on Serpent 2's universal multi-physics interface. Utilizing the multi-physics interface implies that Monte Carlo (MC) code uses the target motion sampling (TMS) method to treat the temperature dependence of the continuous-energy cross sections (Leppänen et al., 2012). TMS has been implemented in Serpent 2 in the recent past (Viitanen and Leppänen, 2012a,b). As off now, unresolved resonances and bound-atom scattering cannot yet be treated with TMS (Viitanen and Leppänen, 2012a, 2013) severely limiting the applicability of the method for nuclear engineering applications. To circumvent this limitation, a fall back to stochastic mixing has been implemented in Serpent 2 to enable the simulation of thermal reactors (Daeubler et al., 2015a).

In its original form the TMS method relies on 0 K continuous energy cross sections and does not require a Doppler Broadening Rejection Correction (DBRC) (Becker et al., 2009; Viitanen and Leppänen, 2012b). One measure to improve the numerical performance of TMS in Serpent is to use a basis library of continuous-energy cross sections for temperatures higher than absolute zero (Viitanen and Leppänen, 2013). However, in the latter case, one has to apply DBRC again. Unfortunately, up to now, the TMS implementation in Serpent 2 is incompatible with DBRC. In this paper, basis continuous-energy cross sections evaluated at 300 K are employed for reasons of computational efficiency but no resonance upscattering is considered.

SUBCHANFLOW as SSS2's thermal-hydraulics module solves three mixture balance equations for mass, momentum and energy in axial direction as well as an additional lateral momentum equation at sub-channel or fuel assembly level (Sanchez et al., 2010). A fully implicit method is used to solve steady-state and transient problems. Three kinds of solvers are available: a direct Gauss elimination solver for small problems, a SOR and a BiCGStab iterative solver. Because of its solution method, SUBCHANFLOW is restricted only to upward flow.

For water material properties and state functions, the IAPWS-IF97 formulations (Cooper, 2007) have been adopted. The heat conduction in a fuel pin is solved with a standard finite volume method. The heat transfer coefficient between fuel pin and reactor coolant is determined by using empirical correlations depending on the heat transfer mode and flow regimes. Void fraction, pressure drop, wall friction and turbulent mixing are also calculated by means of constitutive relations. SUBCHANFLOW is being validated using experimental data relevant for PWR (Imke and Sanchez, 2012), BWR (Jaeger et al., 2013) and liquid metal cooled systems.

SSS2/SCF supports both channel and sub-channel thermal-hydraulics models. After reading and processing its input, the MC neutron transport code automatically prepares the thermal-hydraulic geometry description based on its CSG geometry. There is always a one-to-one correspondence between the feedback meshes Serpent 2 overlays over its 3D geometry to store and lookup feedback information and the numerical meshes of SCF. In a next step, the module SUBCHANFLOW is initialized and executed for the first time in order to obtain an initial guess for distribution of thermal-hydraulic parameters. Thereafter, the Picard iteration is entered. A k-eigenvalue critical source calculation is performed during which heating powers are tallied. The resulting power distribution is passed to SUBCHANFLOW which updates the thermal-hydraulic feedback information. Even though technically possible, the radial dependence of the power production in each fuel pin is currently not modeled due to the excessively large number of neutron histories necessary to obtain statistically significant results. As off now, the MC code's gamma and coupled neutron-gamma transport model is still under development. As a consequence, only pure neutron transport simulations are considered. Furthermore, even though the capability to tally recoil energies from the neutron slowing down process has recently been added to Serpent 2, to keep the first version of the internal coupling simple it is not used for now. Hence, the coolant and structures like fuel rod clads are not heated directly. Accordingly, only effective fuel Doppler, gap and clad temperatures for each rod are provided to Serpent 2 by the sub-channel code. While neither coupled convergence nor the maximum number of coupled iterations have been reached, the solution pattern is repeated. For more technical details on the implementation of SSS2/SCF and the coupled codes assessment, the reader is referred to Daeubler et al. (2015a).

2.3. DYNSUB

In DYNSUB (Daeubler et al., 2015b; Gomez-Torres et al., 2012a, b), the multi-group version of DYN3D released in December 2009 is applied. DYN3D's neutronics solver is able to calculate a detailed multi-group fuel assembly and pin level solution of the neutron transport problem using the diffusion approximation or simplified transport (SP3), based on the developments of Brantley and Larsen (2000).

It applies a multi-group nodal expansion method (NEM) using a quadratic transverse leakage approximation. To treat the time dependency, a fully implicit finite difference scheme using exponential transforms is employed (Beckert and Grundmann, 2008a,b).

In DYNSUB, SUBCHANFLOW acts as thermal-hydraulic module. It has been serially integrated into DYN3D and coupled to neutronics internally. At the end of each steady-state iteration or transient time step, neutronics module updates the (time-dependent) power distribution used as input for the thermal-hydraulics calculation. The thermal-hydraulics module in turn passes fuel pin temperature distributions (radially and axially for each pin), moderator temperatures and densities back to neutronics. In case of a transient calculation, the latter correspond to the values at the end of a time step.

As DYNSUB's cross section update routine only applies one effective Doppler temperature in the look-up and update process per pin cell, the detailed radial fuel temperature distributions for each fuel pin computed by SUBCHANFLOW are condensed into one effective Doppler temperature value. The code offers several possibilities for this condensation.

DYNSUB uses a flexible spatial mapping. An axial thermal-hydraulic mesh layer may correspond to any integer number of axial layers in the neutronics mesh. If DYNSUB is used for pin-homogenized/sub-channel resolved simulations, the neutronic mesh is fuel pin centered but thermal-hydraulics mesh is coolant centered. Simulation results then have to be spatially interpolated before being passed to the other module.

DYNSUB applies the adaptive time step algorithm of DYN3D allowing for having several neutronic time steps inside a thermal-hydraulic one. In terms of coupling numerics for transient simulations, only an explicit marching scheme is available.

A coupled steady-state calculation is considered to be converged when in addition to the internal convergence criteria of the neutronic and thermal-hydraulic codes also convergence criteria on the local Doppler temperature and local moderator density are met. The same set of convergence criteria is used to control the time step size in case of a transient simulation run.

3. Description of the SPERT III E-core

The SPERT III facility is a small thermal research reactor constructed to analyze its dynamic behavior. The E-core was designed to represent a typical commercial PWR (Dugone, 1965). It resembles the latter reactor type in terms of fuel, moderator, coolant flow and system pressure but not its size. Unlike the commercial PWRs, the primary coolant of SPERT III E-core, however, does not contain any soluble boron. Moreover, the core also had a minimal fission product inventory allowing for modeling it with SSS2, SSS2/SCF and DYNSUB without considering fuel depletion.

The radial layout of the SPERT III E-core at the mid plane as modeled with Serpent 2 based on Dugone (1965) is shown in Fig. 1. The core contains a total of 60 fuel assemblies and has an active height of only 97.282 cm. In the core center, one finds the cruciform shaped transient rod (TR) surrounded by four fuel assemblies that contain 16 rods in a 4x4 square array. The blades of the TR are 13.0175 cm wide and 0.476 cm thick. As a whole the TR is 2.3876 m long consisting of two sections. The lower absorber section of the transient rod is made from 1.35 wt% ^{10}B in stainless steel and extends over 96.52 cm. Its upper section is pure stainless steel and is usually in the active core. The 4×4 fuel assemblies are 6.35×6.35 cm square. Their 4.8% enriched UOX fuel rods are placed inside with 1.486 cm pitch. Furthermore, they have an overall length of 1.03632 m and a diameter of 1.184 cm. Both the fuel rod cladding with a thickness of 0.051 cm and the assembly cans are made from stainless steel. The gas gap and plenum in the pins is filled with helium. The UOX fuel pellets have a density of 10.5 $\frac{kg}{m^3}$ and a diameter of 1.067 cm.

The majority of the SPERT III E-core fuel assemblies unlike the ones surrounding the TR contain 25 fuel rods in a canned 5×5 array. These assemblies have the same pin pitch and are made

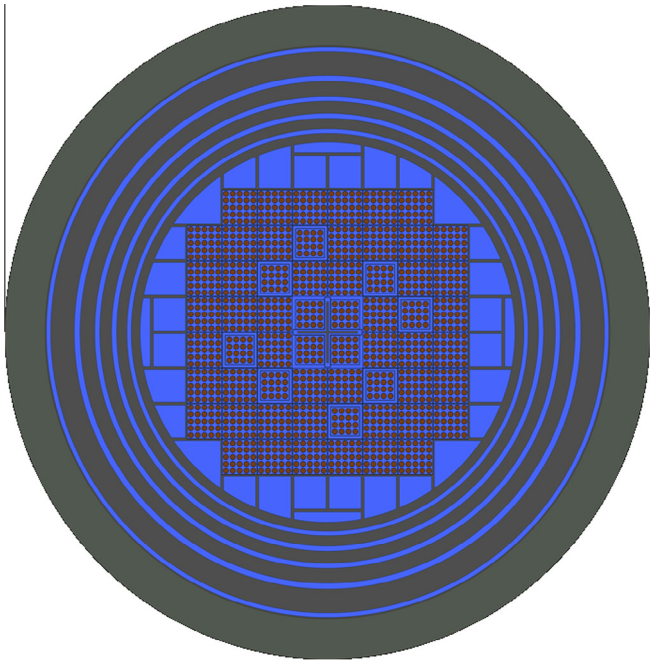

Fig. 1. Radial layout of SPERT III E-core at mid plane as modeled with Serpent 2.

from the same type of fuel rods as their 16-rod counterparts. They are 7.62 × 7.62 cm square.

As seen in Fig. 1,, on top of the 4 × 4 fuel assemblies surrounding the TR eight more are located throughout the reactor core. They are the fuel followers of the eight control rods of the E-core. The poison section of these control rods is square box constructed from a 0.472 cm thick stainless steel plate containing 1.35 wt% ^{10}B. The poison section has a length of 1.168 m and its follower occupies 1.15927 m in axial direction.

Several filler pieces consisting of stainless steel and filled with water hold the 60 fuel assemblies in place inside the reactor core skirt. Between core skirt and the reactor pressure vessel (RPV) wall, there are four thermal shields with water separating them. The active reactor core rests between a bottom and a top support grid both of which are described in detail in Olson (2012). In the RPV, there are water plena below and above the core support structures (Dugone, 1965).

SPERT III's primary system consists of two loops. The primary system and the RPV have been designed for an operating pressure and temperature of 17.33 MPa and 616 K. Each of the loops contains two canned-rotor pumps operating in parallel and a single heat exchanger. The heat removal capacity of the primary system is 60 MW. The E-core, however, has been designed to produce 20 MW under nominal conditions.

The primary coolant enters the RPV at the bottom and passes upward through the active core. In the upper part of the vessel, it reverses direction and flows downwards in the gaps between the thermal shields. The primary coolant exits the RPV near the bottom. For the RIA experiments conducted with the SPERT III E-core (McCardell et al., 1969), all control rods were withdrawn to a position corresponding to the desired reactivity insertion. The reactor is then maintained critical by inserting the poison section of the TR into the lower part of the core. Afterwards, the transient is initiated by accelerating the TR from its initial position out of the core. Its acceleration was measured to be 50.8 $\frac{m}{s^2}$.

The initial operating conditions of the REA tests can be classified into four groups listed in Table 1 (McCardell et al., 1969). For each groups many different reactivity insertions were studied. These

Table 1
Initial conditions for the SPERT III E-core RIA tests.

Initial condition	Coolant inlet T [K]	System pressure [MPa]	Average coolant flow speed [m/s]	Initial reactor power [MW]
Cold startup	294	0.1013	0	0.00005
Hot startup	400/533	10.43	$\leqslant$ 7.3152	0.00005
Hot standby	533	10.43	4.2672	1.0
Operating power	533	10.43	4.2672	20.0

range from delayed super-critical over prompt super-critical into super-prompt critical. A total of 58 accident scenarios were tested.

The experimental data available for all transients of the SPERT III E-core studied are the maximal reactor power, the timing of the power peak, the energy release up to peak power and the reactivity compensation at peak power. For the startup experiments, also the reactor period was determined. Besides these single values, the evolution of core power, reactivity and integral energy release with time has been recorded. The latter data is included in the report (McCardell et al., 1969) as plots whose time scales have been optimized to clearly visualize the shape of the power bursts. As a consequence, this data is only available for a time interval depending on the test case and not over the length of the entire experiment.

The dynamic reactor response was obtained by analyzing reactor power measurements. For these measurements five ex-core uncompensated ^{10}B lined ion chambers were used. The chambers were positioned at different distances from the core. Their current output as a function of reactor power was calibrated using a series of static reactor operation experiments. Cobalt wire activation measurements were carried out for 294 K, 394 K and 478 K coolant inlet temperature. Results had a standard deviation of 15% for reactor power measurements and 17% for energy released.

Furthermore, a number of low- and high-power primary system heat balance experiments were performed with a coolant inlet temperature of 533 K. The one standard deviation spread in the experimental data was 10% for reactor power and 13% for energy released.

For the startup experiments, the reactor period was calculated from the power measurements assuming an initial exponential power rise. To enable a reliable measurement, experiments were designed such that two decades of pure exponential power rise could be observed before the evolution of power being affected by feedback effects. The standard deviation of reactor periods was estimated to be 2%.

For the low initial power RIAs, the inserted reactivity was computed based on the inhour equation of the point kinetic model. To do so, one needs the reactor period, the reduced prompt neutron generation time and delayed neutron parameters. Combining the measurements uncertainties of the contributing quantities one standard deviation for the inserted reactivity is evaluated to be 4%.

For high power tests, it is not possible to measure an undisturbed reactor period. Consequently, the inhour equation was not utilized to determine the inserted reactivity. Instead a control rod worth curve had to be established. The variance of the control worth data from a least-squares fit was used as an uncertainty estimate. Thus, one standard deviation becomes 4%.

The reactivity compensation at peak power was computed employing the point kinetics model. The input quantities are the evolution of reactor power, reduced prompt neutron generation time, reactor period and delayed neutron parameters. Combining the uncertainties of the inputs one standard deviation for the reactivity compensation is about 11%. Since no reactor period measurements can be performed for high power tests, the reactivity compensations quoted for these cases have been approximated

Table 2
Flow area, wetted and heated perimeters for both types of TH channels in SPERT III E-core SCF model.

TH parameter	5 × 5 fuel assembly	4 × 4 fuel assembly
Flow area [cm^2]	27.5086	20.3871
Wetted perimeter [m]	1.22681	0.84144
Heated perimeter [m]	0.92963	0.59496

based on the reactivity over time evolution curves obtained from point kinetics by specifying the steady-state conditions at the beginning of the transient. For these, no estimate of the measurement uncertainty can be made.

4. Numerical SPERT III models

4.1. Serpent 2 and SSS2/SCF static reference models

The Serpent 2 model for the cold startup state covers all of the active reactor core and its supporting structures radially (see Fig. 1) and axially. Below the bottom core support grid another 8 cm of the lower water plenum are considered. ENDF/B VII nuclear data broadened 294 K is employed by SSS2. The Monte Carlo code simulated $4 \cdot 10^5$ neutrons per cycle. 100 inactive cycles were followed by 2000 active ones. Furthermore, the Wielandt shift as a method to accelerate fission source convergence was utilized. For details on the implementation of the Wielandt shift in SSS2, please refer to Daeubler et al. (2015a).

In order to produce a reference solution at operating power conditions with SSS2/SCF, a thermal-hydraulic (TH) model was developed. The SUBCHANFLOW model includes only the active reactor core. The fuel assemblies are represented by single TH channels connecting the lower and upper water plena of the SPERT III RPV. Due the cans of the assemblies these channels are not coupled laterally. The channels' flow area, wetted and heated perimeters are tabulated in Table 2. Each channel is divided into 20 axial nodes.

One effective fuel rod is used to model the all of the fuel pins inside one assembly. For this rod, a radial discretization of 12 nodes to cover fuel (10 nodes), gas gap and clad (2 nodes) is employed. The 4.8 wt% enriched UOX fuel is modeled using SCF's temperature dependent uranium oxide material properties. For the clad, the internal stainless steel property functions were chosen. To approximately model the change of the gas gap heat transfer coefficient with changing reactor and fuel conditions, the Transuranus fuel-clad gap model is enabled in the SCF input. The gamma heating fraction is set to 2.6% – a typical PWR value.

For the hot full power reference model, the coupled code SSS2/SCF utilized ENDF/B VII nuclear data and a 5 K spaced set of thermal scattering data for its stochastic mixing fallback for TMS. Per coupled iteration 300 inactive and 2000 active cycles of $2 \cdot 10^6$ neutrons each were computed. The coupled convergence targets were 5 pcm for the eigenvalue and 0.05% for both Doppler temperature and moderator density. Instead of employing Wielandt's method, the Uniform-Fission-Site (UFS) method available in SSS2 was used for global variance reduction. With this method one tries to increase the number of fission source points in regions, where the fission powers are low in order to decrease statistical uncertainties. In Serpent 2, a regular Cartesian mesh is superimposed on the geometry. In the mesh cells, either collision points, neutron flux or fissions are tallied during the inactive cycles of a calculation. The collected results are used to adjust the number of fission neutrons being emitted in the active cycles. In this work, the adjustment is based on neutron flux tallies.

4.2. Serpent 2 cross section model description

For simulating the SPERT III E-core experiments series with DYNSUB, SSS2 is used as a lattice code to generate homogenized few-group cross section data for the reactor simulator. The SSS2 calculations employed ENDF/B VII nuclear data and produced two-group homogenized group constants. The boundary between the fast and thermal energy group was 0.625 eV. The B1 approximation was enabled in the SSS2 input. With this option, SSS2 uses its tallied homogenized micro-group cross sections to solve the B1 equations. The solution of the latter equations yields the critical spectrum that is then used to re-homogenize the few-group constants for DYNSUB. The micro-group structure used for solving the B1 equations and determining few-group XS is the 44-group structure of one of the SCALE generic XS libraries (ORNL, 2011).

The range and combination of thermal-hydraulic state points included in the XS libraries for DYNSUB for cold startup and operating power conditions are shown in Table 3. The moderator density branches were determined based on the IAPWS-IF97 water/steam tables. Under cold startup and operating power conditions the primary coolant starts to boil at 353 K and 587 K respectively. For these temperatures, four branches considering 20%, 40%, 60% and 80% void are included in both libraries to allow for coolant boiling during severe super-prompt-critical power excursions. By not including moderator temperature branches in the library for DYNSUB, constant pressure conditions are assumed.

The cold start-up library contained six fuel temperature points, whereas the operating power library contained five. Sensitivity studies have shown that including more fuel temperature points in either library did not improve the results. Reducing the number of temperature points, however, led to a decrease in the DYNSUB solution quality.

The spectral geometries used by Serpent 2 for determining few group constants are depicted in Fig. 2. Models shown in subfigure (a) through (d) utilize reflective boundary conditions (BC). To improve DYNSUB's nodal diffusion solution, the fuel assemblies presented in subfigures (a) to (c) assembly discontinuity factors (ADF) are evaluated by Serpent 2. Since the absorber section of the SPERT III E-core CR does not contain any fuel, few group cross sections for it can only be computed by utilizing super cells. The super cell chosen in this work is presented in subfigure (d). For the interface of the CR absorber cell with its fuel assembly neighbors, generalized equivalence theory (GET) interface discontinuity factors (IDF) are produced according to the method developed by Daeubler et al. (2014a). GET IDF are the generalization of ADF for cases where the net neutron currents do not vanish on the boundaries of the cell for which cross sections are to be created.

The cross section calculations were carried out with the model shown in subfigure (a), (c) and (d). They exactly used the branch structure described beforehand. For the central 4 × 4 fuel assemblies, an additional state variable defining the position of the TR (in or out) has to be added to the cross section library.

In the process of developing the cross section libraries for DYNSUB many different models for both the radial and axial reflectors

Table 3
Branch structure of DYNSUB SPERT cross section libraries.

Cold startup		Operating power	
Moderator density [kg/m^3]	Doppler temperature [K]	Moderator density [kg/m^3]	Doppler temperature [K]
998	300	791	533
992	490	762	720
983	720	732	900
972	900	682	1200
958	1200	546	1500
767	1500	409	
575		273	
384		136	
192			

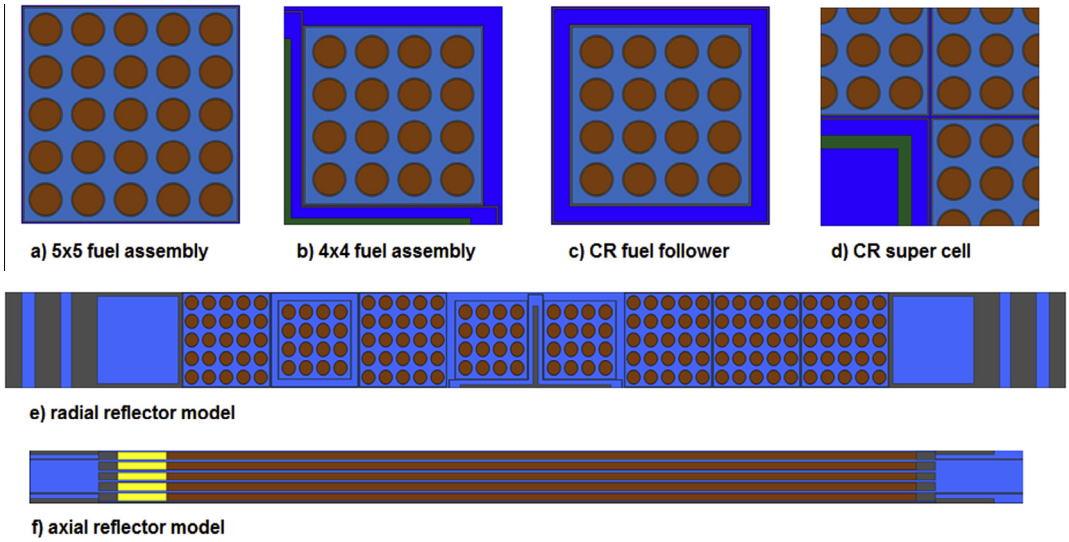

Fig. 2. Spectral geometries used to generate few group cross sections for DYNSUB with Serpent 2.

were tested. The best-performing, final version of both is shown in subfigures (e) and (f) of Fig. 2. The radial reflector model employs vacuum BC in *x*- and reflective BC in *y*-direction. Two cells having the size of a core lattice position describe the active core vicinity in a simplified manner. An analysis of the scalar neutron flux gradients in the SSS2 3D reference model revealed that one may assume vacuum boundary conditions at a distance of two assembly pitches into the reflector. One cell represents the filler pieces between active core and core skirt. The other comprises core skirt and part of the numerous thermal shields. For each reflector cell, one few-group cross section set is generated. Utilizing DYNSUB's newly developed capability to produce IDF, discontinuity factors for both radial reflector few group constant data sets are determined.

The axial reflector model depicted in subfigure (f) is effectively a vertical cut through a 5×5 fuel assembly. Like in the radial reflector case, the *x*-direction BC is vacuum and y-direction one reflection. The bottom axial reflector cross section set describes the foot of the fuel assembly (in subfigure (f) right region not containing orange colored nuclear fuel). The top axial reflector cross section set comprises both the gas plena (yellow) and end plugs of the fuel rods and the fuel assembly head. Since DYNSUB cannot handle discontinuity factors in axial direction at the moment, no IDF for the axial reflectors were computed.

Neither the radial nor the axial reflector cross section sets are branched. It was tested whether considering the effect of the core exit temperature coolant following through gaps between thermal shields had a significant effect. This was not the case. As DYNSUB cannot consider gamma heating, the filler pieces and other structures around the active core are not heated. Thus, there is no need to branch the radial reflector XS. As for the axial reflectors, the bottom reflector is always at inlet conditions. The top reflector mostly sees average reactor coolant heat up corresponding to the SPERT III operating conditions because the majority of RIA transients evolve too quickly to have a significant impact on the coolant properties.

As the few group cross section sets computed for DYNSUB to model SPERT are Monte Carlo neutron transport based estimates, it is important to verify their statistics. In other words: what is the minimum number of neutron histories per transport calculation one needs to simulate with SSS2 such that no inaccuracies caused by undersampling, non-converged fission sources and inter-cycle correlations are propagated into the deterministic reactor simulation by DYNSUB. This question was addressed in a recent publication studying assembly-homogenized two-group cross sections and ADF for 17×17 Westinghouse PWR fuels (Kaltiaisenaho and Leppänen, 2014). For both fuel assemblies, a total of 50 million neutron histories proved to sufficient. Thus, to compute the SPERT cross sections for the spectral geometries shown in subfigures (a) to (d) in Fig. 2 SSS2 simulated 25,000 neutrons per cycle in 2000 active cycles for each transport run. 300 cycles were skipped. For the two reflector models, the analysis of Kaltiaisenaho and Leppaenen is not applicable. As a result, the number of neutron histories simulated here was chosen conservatively. SSS2 ran the same number of cycles as for the other models but employed 50,000 neutrons in each cycle. Furthermore, to ensure the reflector regions were well populated Wielandt's method was enabled.

The lattice calculations for the cold startup cross section library took 47.0 h on a dual socket Intel Xeon E5-2697 v2 with 379 GB of host memory running Mageia release 4×64. The SSS2 calculation was performed using 48 threads. The corresponding simulations for the operating power library consumed 64.5 h on the same machine using an identical number of threads. Based on these numbers it is clear that computational cost of Monte Carlo based homogenization is significantly higher than that of classical deterministic lattice codes. However, it is within the capability of small modern parallel computers to finish SSS2 lattice calculations for cases like the SPERT III experiments in an acceptable amount of time. This finding is in line with the conclusion on the practical feasibility of Monte Carlo neutron based spatial homogenization drawn by Leppänen and Mattila (2014).

4.3. DYNSUB steady-state and transient model

In the DYNSUB model, the SPERT III E-core is represented by 140 radial nodes, 60 of which are fuel assemblies, and 80 are radial reflectors forming two complete rings around the active core. Axially, 100 equidistant mesh layers describe the axial extend of the fuelled region. Another 14 and 19 mesh layers are utilized to simulate the bottom and top axial reflectors respectively. The high axial resolution employed in the DYNSUB model was chosen to capture the fast movement of the TR and the corresponding reactivity insertion as accurately as possible. The axial and radial boundary conditions are zero neutron flux.

The two-group diffusion cross section libraries produced with Serpent 2 presented in the last subsection are utilized. For the SPERT E-core experiments series, a new DYNSUB cross section table type was developed. Unlike all previously existing XS tables,

Table 4
Overview of initial conditions of the eight selected SPERT III E-core RIA tests.

Test no.	Initial reactivity insertion [$]	Coolant inlet temperature [K]	Coolant flow speed [m/s]	Reactor power [MW]	System pressure [MPa]
Cold startup					
18	0.90 ± 0.04	294.3 ± 2.2	0.0	0.00005	0.1013
49	1.00 ± 0.04	297.6 ± 2.2	0.0	0.00005	0.1013
43	1.21 ± 0.05	298.7 ± 2.2	0.0	0.00005	0.1013
Hot standby					
79	0.86 ± 0.03	540.4 ± 2.2	4.2672	1.1 ± 0.1	10.43
81	1.17 ± 0.04	535.4 ± 2.2	4.2672	0.9 ± 0.1	10.43
82	1.29 ± 0.04	535.9 ± 2.2	4.2672	1.2 ± 0.1	10.43
Operating power					
85	0.87 ± 0.04	534.8 ± 2.2	4.2672	19.0 ± 1.0	10.43
86	1.17 ± 0.05	534.3 ± 2.2	4.2672	19.0 ± 1.0	10.43

this one considers the dependence of both the effective delayed neutron fraction and the delayed neutron decay constants of the six delayed neutron precursor families on the thermal-hydraulic state.

The thermal-hydraulics model used by DYNSUB is identical to the one of SSS2/SCF except that it discretizes the axial height of the core with 100 mesh layers. The convergence criteria used for the steady-state simulations are $\epsilon_{keff} < 10^{-5}$ for the eigenvalue, $\epsilon_{DT} < 10^{-4}$ for local Doppler temperature and $\epsilon_{RM} < 10^{-4}$ for the local moderator density.

Before turning to modeling the REA experiments, DYNSUB is employed to perform stationary simulations of the SPERT III E-core under cold startup and operating power conditions. DYNSUB results are compared to the Serpent 2 and SSS2/SCF reference solutions in order to evaluate the quality of the developed multi-dimensional cross section tables and the DYNSUB nodalization.

As mentioned in Section 3,, a total of 58 RIA experiments were performed for the SPERT III E-core. It is out of the scope of this paper to analyze all of these experiments in detail. Hence, eight transients starting from cold startup, hot standby and operating power conditions were selected. The hot standby REAs can be modeled using the operating power cross section libraries. For each initial condition, the cases to be studied were chosen such that they include at least one delayed super-critical and one super-prompt critical scenario. Whenever possible, a prompt super-critical case was considered. The initial conditions of the selected tests are listed in Table 4 (McCardell et al., 1969).

Unfortunately, for none of the 58 REAs the initial positions of the TR and eight CRs of the SPERT III E-core are specified in the experimental documentation (McCardell et al., 1969). Only the system pressure, coolant inlet temperature, coolant flow speed, reactor power and initial reactivity insertion are known. Therefore, the first step in any DYNSUB transient analysis is to position the TR such that its static worth matches the known initial reactivity insertion. The CRs are withdrawn from the core to keep it critical. At the beginning of the transient simulation, the TR is then accelerated towards the bottom of the active core until it is fully withdrawn. For all eight RIA calculations, DYNSUB employs a fixed time step of 0.1 ms as sensitivity tests confirmed that this leads to a time-converged solution in all cases.

5. Stationary simulations of the SPERT III E-core

5.1. Cold zero power

For the SPERT III E-core experiment series, no detailed steady-state measurements are included in the experimental report (McCardell et al., 1969). The only quoted measured properties of the E-core under cold startup conditions mentioned in the report are compared with simulation results obtained with Serpent 2 and DYNSUB in Table 5.

The Monte Carlo code captures the experimentally determined control rod position quite well. The reactor eigenvalue predicted by SSS2 for the measured critical CR position is 0.99702 ± 0.00004. The critical CR position computed by DYNSUB is significantly further off but in line with other deterministic assembly-homogenized models such as the CASMO5/SIMULATE-3K qualification model (Grandi and Moberg, 2012). The latter evaluated the SPERT III E-core to be critical with the CR tips positioned at 30.1 cm.

The experimental report mentions that the excess reactivity of the E-core is 14 $. Given the reactivity measurement uncertainties discussed in Section 3, both SSS2 and DYNSUB reproduce the experimental data within one standard deviation (0.56 $). For the worth of the TR, the Serpent 2 result only falls within two standard deviations of the measurement. DYNSUB's prediction, however, differs by less than a standard deviation.

Unlike SSS2, DYNSUB cannot compute the reduced generation time. The value obtained with the Monte Carlo code matches the experiment perfectly. In the SPERT report, no information on the uncertainty of the reduced generation time evaluation was found.

In order to test the cold startup cross section library and the DYNSUB model further, a more detailed comparison between the SSS2 reference results and the DYNSUB nodal diffusion predictions were carried out. With the eight control rods and the transient rod withdrawn from the core, the effective multiplication factor determined by Serpent 2 becomes 1.11454 ± 0.00004. DYNSUB evaluates the same factor to be 1.11106 which is 438.4 pcm less. When comparing low order deterministic transport to high order reference solution differences of this magnitude are expected. For example, in the OECD/NEA and U.S. NRC PWR MOX/UO2 core transient benchmark the differences in eigenvalue between the 47G MOC DeCART reference and nodal solutions are of the same order of magnitude (Kozlowski and Downar, 2007).

In a next step, the relative differences in assembly power evaluated with Serpent 2 and DYNSUB have been determined and are visualized in Fig. 3. The maximal difference in assembly power is below 3.4% everywhere. Serpent 2 predicts power to be generated in the fuel assemblies to be higher than that of DYNSUB in most of the fuel assemblies near the core periphery and in the four 4x4 fuel assemblies surrounding the TR. As can be seen in Fig. 4 the production of power in the DYNSUB model is slightly more shifted to the lower half of the core than in the SSS2 calculation. This is consistent with the reported difference in critical control rod position between the two reactor simulators. But generally an acceptable agreement in terms of axial power profiles is observed.

5.2. Hot operating power

After looking at a cold startup steady-state which is essentially a pure neutronics problem, the assessment of the Serpent 2-DYNSUB code sequence is continued by including thermal hydraulic feedback, i.e. analyzing a steady-state at operating power. SSS2/SCF reference solution of the all rods out state converged after five

Table 5
Comparison of integral quantities computed with SSS2 and DYNSUB with corresponding cold startup measurements.

Quantity	Measured	SSS2	DYNSUB
Critical CR position	37.084 cm	37.719 cm	30.1498 cm
Excess reactivity	14 $	14.21 $	13.7 $
TR worth	4.8 $	4.54 $	4.67 $
Reduced generation time	2.15 ms	2.15 ms	

	A	B	C	D	E	F	G	H
1		-0.69	2.88	2.67	2.94	3.39	-0.54	
2	-0.54	1.50	-0.35	-0.79	0.29	-0.12	1.50	-0.69
3	3.39	-0.13	-1.32	-2.87	-2.65	-1.32	-0.34	2.88
4	2.94	0.29	-2.65	2.11	2.12	-2.87	-0.79	2.69
5	2.69	-0.78	-2.87	2.11	2.11	-2.64	0.29	2.94
6	2.89	-0.35	-1.32	-2.64	-2.87	-1.32	-0.12	3.39
7	-0.69	1.50	-0.12	0.30	-0.79	-0.35	1.50	-0.54
8		-0.54	3.39	2.95	2.69	2.89	-0.69	

Fig. 3. Relative differences in SPERT assembly powers in per cent between SSS2 and DYNSUB under cold startup conditions.

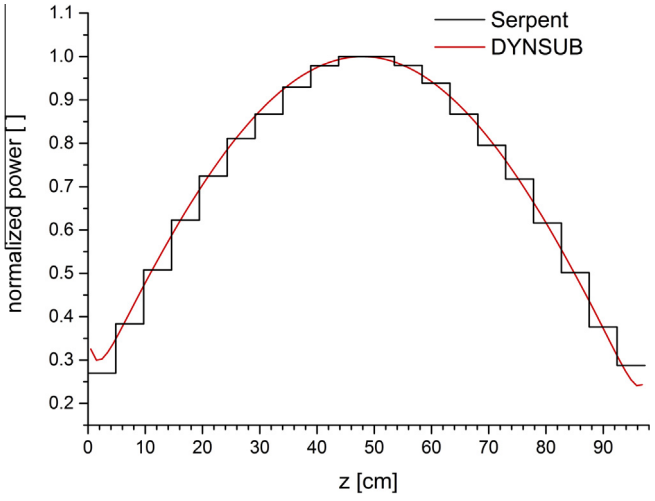

Fig. 4. SPERT cold startup axial power profiles as computed by SSS2 and DYNSUB.

coupled iterations. The eigenvalue determined with the Monte Carlo neutron transport based tool is 1.04041 ± 0.00001. DYNSUB's value of 1.041319 closely matches the high order prediction by only overestimating core multiplication by 90.9 pcm.

While enabling thermal-hydraulic feedback decreased the differences in eigenvalue, the maximal difference in fuel assembly power is increased to almost 6% in the corner assemblies at the core periphery (see Fig. 5). The assembly powers computed with SSS2/SCF are higher than DYNSUB results in almost all fuel assemblies except for the corner fuel assemblies at the core periphery and eight fuel assemblies surrounding the central 4 × 4 fuel.

Like for the cold startup case, the axial power profile evaluated using DYNSUB is slightly more bottom peaked than the one determined with SSS2/SCF as Fig. 6 shows. The axial dependence of the radially averaged fuel Doppler temperatures computed with both reactor simulators generally follows the same gross trends as the axial power profiles except that DYNSUB's predictions are slightly higher than SSS2/SCF's (cp. Fig. 7).

This is due to the differences in the radial power profiles. The eight fuel assemblies for which DYNSUB overpredicts the powers near the center of the SPERT III E-core are by far the hottest. In the SSS2/SCF reference solution, the neighbors of these fuel assemblies have Doppler temperatures that are more than 100 K smaller than those of the assemblies themselves. The difference in Doppler temperatures between the core periphery and these eight assemblies is over 300 K.

Even though DYNSUB underestimates the power produced in most of the other colder fuel assemblies, the lower Doppler temperature predictions in them cannot counteract the large contribution from the eight fuel assemblies near the core center to the radial Doppler temperature average.

The radially averaged heat up of the primary coolant as evaluated by SSS2/SCF and DYNSUB was found to be in good agreement considering the differences in radial power distributions and the convergence limits of the Monte Carlo thermal-hydraulics reference (see Fig. 8).

5.3. Summary of stationary SPERT III E-core calculations

Considering that DYNSUB's solutions were obtained with a 2G nodal diffusion neutronics model, the observed agreement with the Monte Carlo neutron transport based reference computations for cold startup and operating power conditions is satisfactory indicating that the Serpent 2-DYNSUB code sequence has been set up correctly for stationary problems. More importantly, the comparison for the latter conditions proves that the newly introduced Serpent 2 automatic branching capability for calculating multi-dimensional few-group cross section tables functions properly. The operating power steady-state simulation can be viewed as the first successfully completed solution verification case for the cross section generation methodology of Serpent 2 as a whole for hot full power condition problems.

6. Simulation of selected SPERT III E-core reactivity-initiated accident tests

A summary of the DYNSUB transient results for cold startup initial conditions compared to documented measured data is presented in Table 6. Values obtained with DYNSUB written in bold are not within one standard deviation of the experimentally determined values. All other computed data is within one standard deviation.

For all RIAs starting from cold startup conditions the reactor periods computed based on DYNSUB simulations are bigger than the experimentally obtained ones but they follow the same trends. Also cold startup reactor periods determined with CASM05/SIMULATE-3K did not agree with the measured data within one standard deviation for many RIA tests (Grandi and Moberg,

	A	B	C	D	E	F	G	H
1		-5.91	0.23	0.45	0.68	0.56	-5.85	
2	-5.79	1.60	0.81	0.50	2.25	0.54	1.59	-5.95
3	0.63	0.64	0.70	-1.50	-1.46	0.69	0.76	0.25
4	0.67	2.28	-1.46	3.48	3.47	-1.52	0.46	0.39
5	0.42	0.43	-1.47	3.49	3.51	-1.49	2.31	0.73
6	0.25	0.76	0.72	-1.42	-1.49	0.69	0.65	0.58
7	-5.93	1.58	0.67	2.28	0.47	0.79	1.60	-5.82
8		-5.85	0.66	0.74	0.42	0.24	-5.95	

Fig. 5. Relative differences in SPERT assembly powers in per cent between SSS2/SCF and DYNSUB under operating power conditions.

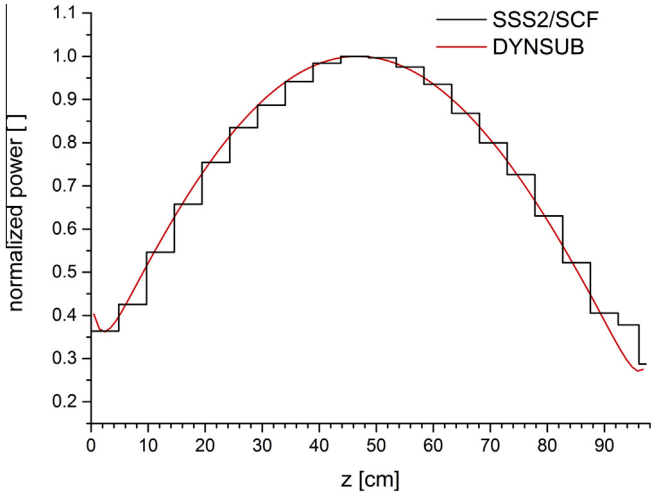

Fig. 6. SPERT operating power axial power profiles as computed by SSS2/SCF and DYNSUB.

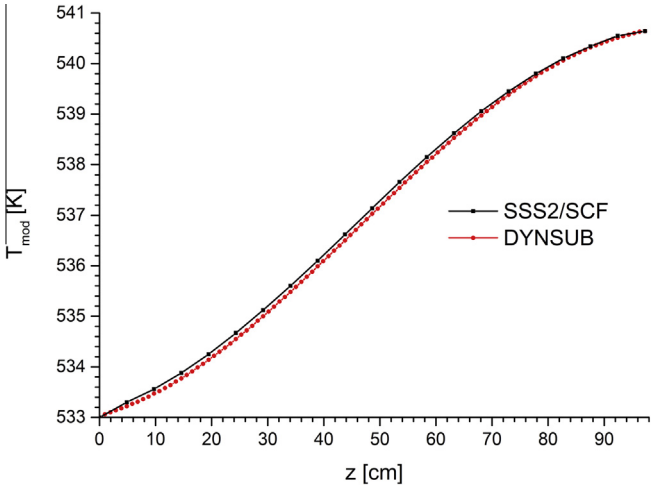

Fig. 8. SPERT operating power radially averaged moderator temperature profiles as evaluated by SSS2/SCF and DYNSUB.

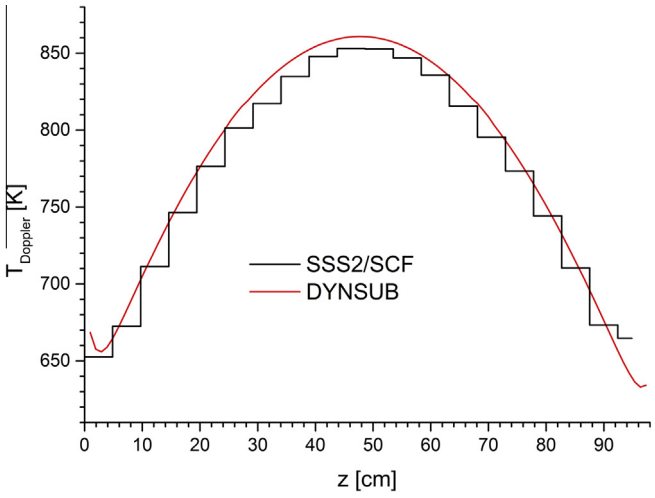

Fig. 7. SPERT operating power radially averaged Doppler temperature profiles as determined with SSS2/SCF and DYNSUB.

2012). Furthermore, if one considers that for cold startup RIA tests with the same initial reactivity insertion, i.e. test 19 and 20, the measured reactor period deviated by 9 ms even though the quoted uncertainty of the measurement is less than 1 ms in both cases (McCardell et al., 1969), DYNSUB's performance is acceptable.

The evolution of SPERT III reactor power and reactivity for the delayed super-critical test 18 are depicted in Fig. 9. DYNSUB's reactivity prediction follows the experimentally determined curve closely. After an initial very good agreement between the simulated reactor core power and the measured one (up to 3.5 s into the transient), the computed values start to deviate once thermal-hydraulic feedback starts to play a significant role. While the overall shape of the delayed super-critical power peak is similar to the experiment the maximal power computed with DYNSUB is 5.08 MW instead of 4.3 ± 0.6 MW. While the original experiments were carried without any primary coolant flow (see Table 4), DYNSUB cannot simulate such an experimental condition due to a limitation of SUBCHANFLOW. The coolant flow was set to a small value, i.e. 1 kg/s. The addition of some forced convection improves the cooling of the SPERT III E-core in the DYNSUB model reflected in the overestimation of peak power. Due to the design of the

Table 6
Summary of the DYNSUB simulation results for selected cold startup RIA tests.

Test no.		Initial reactivity [$]	Max. power [MW]	Peak time [s]	Energy release [MJ]	Reactivity compensation [$]	Reactor period [ms]
18	Exp.	0.90 ± 0.04	4.3 ± 0.6	5.3 ± 0.1	6.7 ± 1.1	0.23 ± 0.03	351 ± 7
	DYNSUB	0.879	**5.08**	5.36	7.8	0.226	**360.2**
49	Exp.	1.00 ± 0.04	11.0 ± 2.0	0.97 ± 0.04	2.1 ± 0.4	0.08 ± 0.01	68.4 ± 1.4
	DYNSUB	1.02	**13.09**	1.003	**2.56**	0.0835	**74.6**
43	Exp.	1.21 ± 0.05	280 ± 42	0.230 ± 0.006	6.0 ± 1.0	0.22 ± 0.02	10.0 ± 0.2
	DYNSUB	1.20	284.48	0.231	6.65	0.228	**11.4**

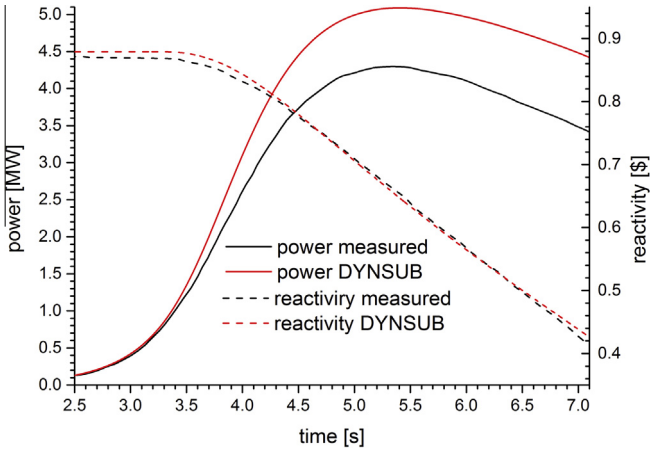

Fig. 9. DYNSUB core power and reactivity results for cold startup test 18.

SPERT RPV (see Section 3) natural circulation cannot establish itself and plays no role in the cold startup experiments.

Fig. 10 shows the DYNSUB core power and reactivity evolution for the prompt super-critical cold startup test 49. As expected, the power excursion happens significantly faster and a peak is reached after 1.0 s. Just as for test 18, the measured and computed core reactivity match well. DYNSUB once more overestimates the height of the power peak. Like for the delayed super-critical case, this is partially due to the small coolant flow modeled in DYNSUB.

The last cold startup REA experiment studied with DYNSUB is a super-prompt critical power excursion that is characterized by a reactor period as short as 10.0 ms in its initial phase. The core power and reactivity evaluated using DYNSUB are contrasted with measurements in Fig. 11. The DYNSUB model captures the power peak well both in terms of shape and height. Differences between calculated and measured reactivities in the later phase of the transient are mostly due to the fact that DYNSUB computed dynamic reactivities employing adjoint fluxes while the experimental values were inferred from reactor power and period measurements using point kinetics.

Under hot standby conditions, all DYNSUB simulations predict the measured data within one standard deviation as can be seen in Table 7. As seen in Figs. 12–14, the DYNSUB transient computations are generally in good agreement with the measured evolution of reactor power and reactivity in time. For two super-prompt critical RIAs, test 81 and 82, the power level after the peak determined with DYNSUB is higher than measurements. Sensitivity studies performed identified the fuel-clad gap model to have the largest impact on the simulation results in this phase of the transients. Of the models available in SUBCHANFLOW the Transuranus model performed best. However, there is room for further improvement.

For test 81 and 82, the reactivity insertion modeled with DYNSUB in the early phase of the transient differs from the measured behavior. However, it has to be kept in mind that the experimental reactivities were computed from reactor power measurements using point kinetics. Due to the fact that reactivity compensation already occurs early during the on-going reactivity insertion for these RIAs no reactor period could be obtained experimentally. Hence, the point kinetic based reactivity evaluation had to use computed concentrations of the delayed neutron precursors as initial conditions.

For both RIAs starting from operating power conditions analyzed with DYNSUB, the reactor simulator only failed to determine the energy released within one standard deviation in test 85 (see Table 8). For easier analysis, the corresponding simulation result is written in bold face in Table 8. For completeness, the change

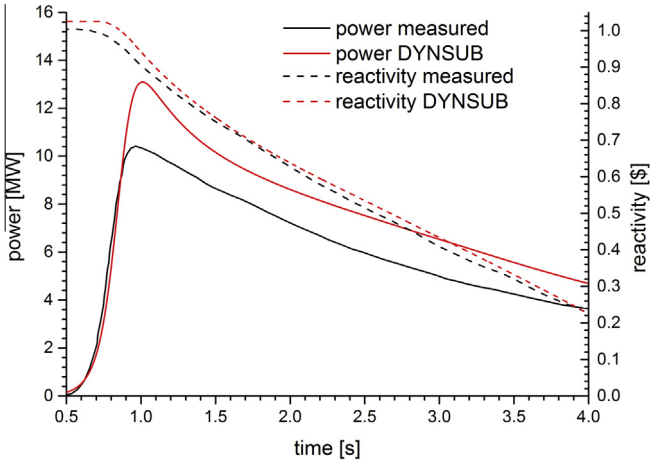

Fig. 10. DYNSUB core power and reactivity results for cold startup test 49.

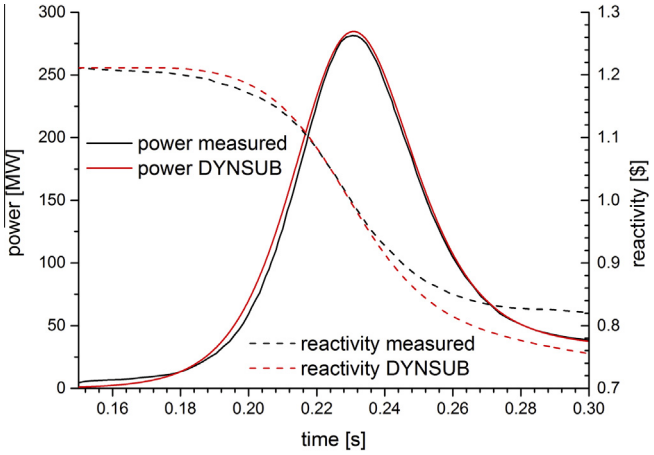

Fig. 11. DYNSUB core power and reactivity results for cold startup test 43.

Table 7
Summary of the DYNSUB simulation results for selected hot standby RIA tests.

Test no.		Initial reactivity [$]	Max. power [MW]	Peak time [s]	Energy release [MJ]	Reactivity compensation [$]
79	Exp.	0.86 ± 0.03	13.0 ± 1.0	0.68 ± 0.08	6.7 ± 0.9	0.09
	DYNSUB	0.856	13.34	0.751	7.34	0.092
81	Exp.	1.17 ± 0.04	330 ± 30	0.135 ± 0.003	7.8 ± 1.0	0.180
	DYNSUB	1.16	324.90	0.138	8.20	0.181
82	Exp.	1.29 ± 0.04	880 ± 90	0.118 ± 0.002	15.0 ± 2.0	0.30
	DYNSUB	1.293	871.50	0.120	13.70	0.306

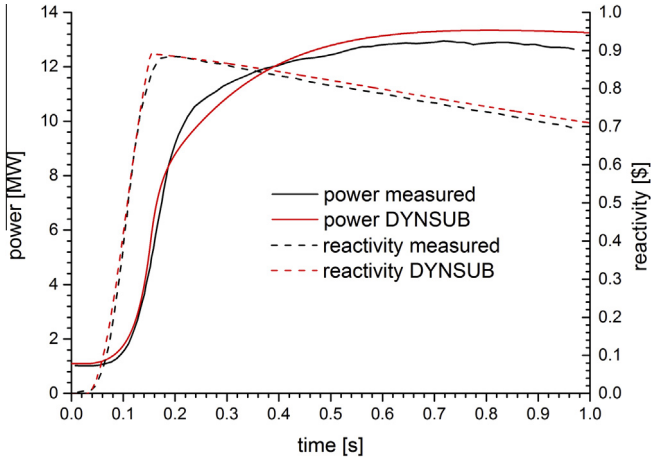

Fig. 12. DYNSUB core power and reactivity results for hot standby test 79.

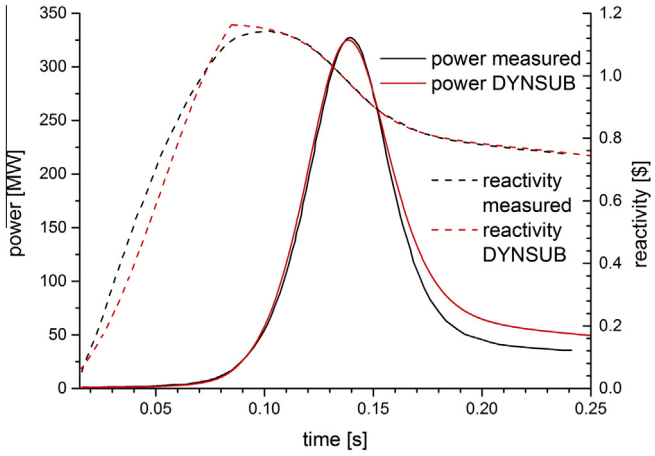

Fig. 13. DYNSUB core power and reactivity results for hot standby test 81.

of SPERT III E-core power and reactivity as predicted by DYNSUB is compared to measured curves in Figs. 15 and 16.

7. Conclusion and outlook

The objective of the work presented in this paper was to validate the Serpent 2-DYNSUB code utilizing the SPERT III E-core experiment series. The Serpent 2 and SSS2/SCF numerical reference models as well as the coupled DYNSUB and Serpent 2 cross section generation models were developed using data from the original SPERT experimental reports (Dugone, 1965; McCardell et al., 1969). The DYNSUB stationary simulations compared well to the Monte Carlo neutron transport reference solutions obtained with Serpent 2 (cold startup conditions) and SSS2/SCF (operating power conditions). With the latter MC/TH reference, the cross section calculation methodology of Serpent 2 was verified for the first time for operating conditions other than HZP.

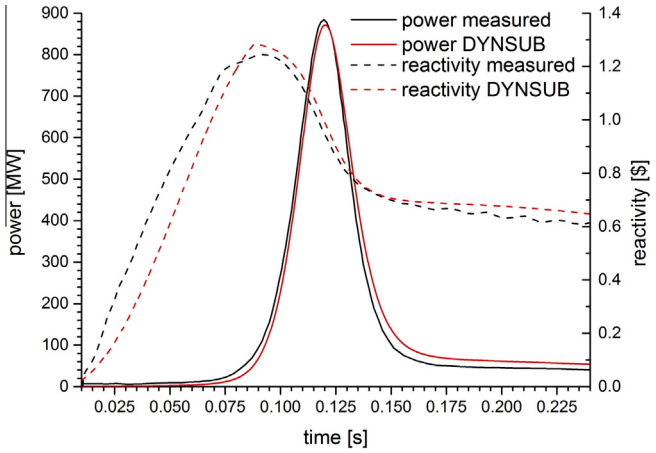

Fig. 14. DYNSUB core power and reactivity results for hot standby test 82.

The nodal diffusion DYNSUB simulations of eight selected experiments were generally in good agreement with measurements. As the selected experiments cover much of the possible transient (delayed super-critical, prompt super-critical and super-prompt critical excursion) and initial conditions (cold and hot as well as zero, little and full power reactor states) one expects in commercial PWRs, the obtained results give confidence that DYNSUB employing nodal diffusion is suitable to model REAs and other RIAs in PWRs.

Furthermore, the successful application of the Serpent 2-DYNSUB code sequence to model the SPERT III E-core RIA tests underlines that the Serpent 2 methodology to determine homogenized few-group constants not only works fine under hot full power conditions but also for RIA transients starting from various initial conditions. The study presented in this chapter is additionally a validation of Serpent 2's methods to evaluate neutron kinetic parameters for reactor simulators like DYNSUB.

In the future, the remainder of the 58 SPERT III E-core RIA tests is to be analyzed with DYNSUB to complete the Serpent 2-DYNSUB validation base. Afterwards, validation efforts are to be repeated for nodal DYNSUB calculations using the simplified transport solver and pin-homogenized DYNSUB simulations employing both the diffusion and simplified transport approximations. Since DYNSUB offers multi-group solutions for any of its neutronics solvers, work on optimizing the few group energy structure of the cross sections for the SPERT III E-core should be carried out.

Last but not least, to complete the verification, validation and uncertainty quantification (VVUQ) process of the Serpent 2-DYNSUB code sequence for REAs, a formal sensitivity and uncertainty analysis of the results is to be done. This should be based on the uncertainty quantification methods established in the framework of the OECD UAM benchmark (Ivanov et al., 2007).

Table 8
Summary of the DYNSUB simulation results for selected operating power RIA tests.

Test no.		Initial reactivity [$]	Max. power [MW]	Peak time [s]	Energy release [MJ]	Reactivity compensation [$]
85	Exp.	0.87 ± 0.04	130 ± 10	0.155 ± 0.005	8.7 ± 1.1	0.04
	DYNSUB	0.868	121.5	0.135	**7.5**	0.039
86	Exp.	1.17 ± 0.05	610 ± 60	0.110 ± 0.005	17.0 ± 2.0	0.22
	DYNSUB	1.17	607.2	0.107	16.17	0.22

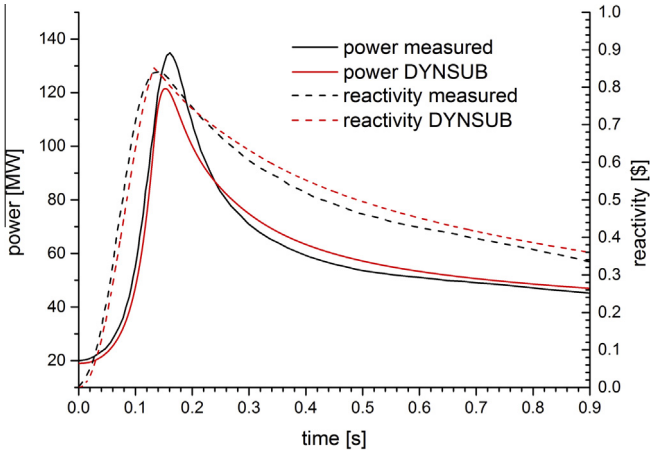

Fig. 15. DYNSUB core power and reactivity results for operating power test 85.

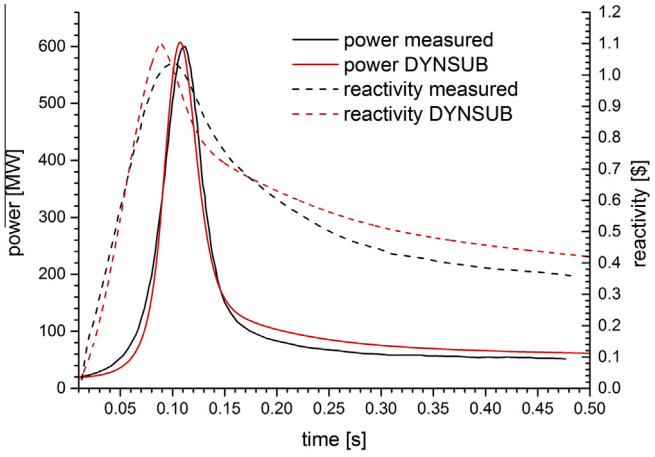

Fig. 16. DYNSUB core power and reactivity results for operating power test 86.

Acknowledgements

The authors wish to acknowledge the support of the Nuclear Safety Program for the research topic "multi-physics methods for LWR" and the Steinbuch Centre for Computing (SCC) of the Karlsruhe Institute of Technology (KIT). Additionally, the authors thank VTT Technical Research Center of Finland for their assistance concerning the Serpent 2 code.

References

Aoki, S., Suemura, T., Ogawa, J., Takeda, T., 2009. Analysis of the SPERT-III E-Core using ANCK code with chord weighting method. Nucl. Sci. Technol. 46, 239–251.

Becker, B., Dagan, R., Lohnert, G., 2009. Proof and implementation of the stochastic formula for ideal gas, energy dependent scattering kernel. Ann. Nucl. Energy 36, 470–474. http://dx.doi.org/10.1016/j.anucene.2008.12.001.

Beckert, C., Grundmann, U., 2008a. Development and verification of a nodal approach for solving the multigroup SP3 equations. Ann. Nucl. Energy 35, 75–86.

Beckert, C., Grundmann, U., 2008b. Entwicklung einer Transportnaeherung fuer das reaktordynamische Rechenprogramm DYN3D. Technical Report. Research Center Dresden-Rossendorf.

Brantley, P.S., Larsen, E., 2000. The simplified P3 approximation. Nucl. Sci. Eng. 134, 1–12.

Cooper, J. et al., 2007. Revised release on the iapws industrial formulation 1997 for the thermodynamic properties of water and steam. Technical Report. International Association for the Properties of Water and Steam.

Daeubler, M., Jimenez, J., Sanchez, V., 2014a. Generation and application of interface discontinuity factors in the reactor simulator DYN3D. In: Proceedings of ICAPP 2014, Charlotte, North Carolina.

Daeubler, M., Ivanov, A., Sjenitzer, B.L., Sanchez, V., Stieglitz, R., Macian-Juan, R., 2015a. High-fidelity coupled Monte Carlo neutron transport and thermal-hydraulic simulations using Serpent 2/SUBCHANFLOW. Ann. Nucl. Energy 83, 352–375.

Daeubler, M., Trost, N., Jimenez, J., Sanchez, V., Stieglitz, R., Macian-Juan, R., 2015b. Static and transient pin-by-pin simulations of a Full PWR core with the extended coupled code system DYNSUB. Ann. Nucl. Energy 84, 31–44.

Dugone, J., 1965. SPERT III reactor facility: E-core revision. Technical Report IDO-17036. U.S. Atomic Energy Commission.

Fridman, E., Leppänen, J., 2011. On the use of the Serpent Monte Carlo code for few-group cross section generation. Ann. Nucl. Energy 38, 1399–1405.

Gomez-Torres, A.M., Sanchez-Espinoza, V.H., Ivanov, K., Macian-Juan, R., 2012a. DYNSUB: A high fidelity coupled code system for the evaluation of local safety parameters – Part I: development, implementation and verification. Ann. Nucl. Energy 48, 108–122. http://dx.doi.org/10.1016/j.anucene.2012.05.011.

Gomez-Torres, A.M., Sanchez-Espinoza, V.H., Ivanov, K., Macian-Juan, R., 2012b. DYNSUB: A high fidelity coupled code system for the evaluation of local safety parameters – Part II: comparison of different temporal schemes. Ann. Nucl. Energy 48, 123–129. http://dx.doi.org/10.1016/j.anucene.2012.05.033.

Grandi, G., 2014. Validation of CASMO5/SIMULATE-3K using the special power excursion test reactor E-core: cold start-up, hot start-up, hot standby and full power conditions. In: Proceedings of PHYSOR 2014 conference.

Grandi, G., Moberg, L., 2012. Qualification of CASMO5/SIMULATE-3K against the SPERT-III E-core cold start-up experiments. In: Proceedings of PHYSOR 2012 conference.

Imke, U., Sanchez, V., 2012. Validation of the subchannel code SUBCHANFLOW using NUPEC PWR tests (PSBT). Sci. Technol. Nucl. Installations, 1–12.

Ivanov, K., Avramova, M., Kodeli, I., Sartori, E., 2007. Benchmark for Uncertainty Analysis in Modeling (UAM) for design, operation and safety analysis of LWRs. Technical Report NEA/NSC/DOC(2007) 23. OECD Nuclear Energy Agency/Nuclear Science Committee.

Jaeger, W., Manes, J.P., Imke, U., Jimenez, J., Sanchez, V., 2013. Comparison of two-phase flow modeling capabilities of CFD, sub channel and system codes by means of post-test calculations of BFBT transients. Nucl. Eng. Des. 263, 313–326.

Kaltiaisenaho, T., Leppänen, J., 2014. Analysing the statistics of group constants generated by Serpent 2 Monte Carlo code. In: Proceedings of PHYSOR 2014 conference.

Kozlowski, T., Downar, T.J., 2007. OECD/NEA AND U.S. NRC PWR MOX/UO2 CORE TRANSIENT BENCHMARK – Final Report. Technical Report. OECD Nuclear Energy Agency/Nuclear Science Committee.

Leppänen, J., 2009. Two practical methods for unionized energy grid construction in continuous-energy Monte Carlo neutron transport calculation. Ann. Nucl. Energy 36, 878–885. http://dx.doi.org/10.1016/j.anucene.2009.03.019.

Leppänen, J., 2013a. Development of a dynamic simulation mode in Serpent 2 Monte Carlo Code. In: Proceedings of M&C 2013 conference, Sun Valley, Idaho.

Leppänen, J., 2013b. Serpent a continuous-energy Monte Carlo reactor physics burnup calculation code. Technical Report. VTT Technical Research Centre of Finland.

Leppänen, J., 2014. Methodology for spatial homogenization in Serpent 2. Technical Report. VTT Technical Research Centre of Finland.

Leppänen, J., Mattila, R., 2014. On the practical feasibility of continuous-energy monte carlo in spatial homogenization. In: Proceedings of PHYSOR 2014 conference.

Leppänen, J., Viitanen, T., Valtavirta, V., 2012. Multi-physics coupling scheme in the Serpent 2 Monte Carlo code. Trans. Am. Nucl. Soc. 107, 1165–1168.

Leppänen, J., Mattila, R., Pusa, M., 2014a. Validation of the Serpent-ARES code sequence using the MIT BEAVRS benchmark – initial core at HZP conditions. Ann. Nucl. Energy 69, 212–225.

Leppänen, J., Pusa, M., Viitanen, T., Valtavirta, V., Kaltiaisenaho, T., 2015. The Serpent Monte Carlo code: status, development and applications in 2013. Ann. Nucl. Energy 82, 142–150.

McCardell, R., Herborn, D., Houghtaling, J., 1969. Reactivity accident test results and analysis for the SPERT III E-core – A small oxide-fueled, pressurized-water reactor. Technical Report IDO-17281. U.S. Atomic Energy Commission.

Olson, A.P., 2012. Innovative methods for research reactors, SPERT III E-core reactor specification. Technical Report. International Atomic Energy Agency CRP.

ORNL, 2011. Scale: a comprehensive modeling and simulation suite for nuclear safety analysis and design. Technical Report ORNL/TM-2005/39.

Sanchez, V., Imke, U., Ivanov, A., Gomez, R., 2010. SUBCHANFLOW: a thermal-hydraulic sub-channel program to analyse fuel rod bundles and reactor cores. In: Proceedings of the 17th Pacific Basin Nuclear Conference.

Viitanen, T., Leppänen, J., 2012a. Explicit temperature treatment in the Monte Carlo neutron tracking routines first results. In: Proceedings of PHYSOR 2012 conference, Knoxville, Tennessee.

Viitanen, T., Leppänen, J., 2012b. Explicit treatment of thermal motion in continuous-energy Monte Carlo tracking routines. Nucl. Sci. Eng. 171, 165–173, dx.doi.org/10.13182/NSE11-36.

Viitanen, T., Leppänen, J., 2013. Optimizing the implementation of the target motion sampling temperature treatment technique how fast can it get?. In: Proceedings of M&C 2013 conference, Sun Valley, Idaho.

Wang, R.C., Xu, Y., Hudson, N., Downar, T.J., 2013. Validation of the U.S. NRC coupled code system TRITON/TRACE/PARCS using the Special Power Excursion Reactor Test III. Nucl. Technol. 183, 504–514.

Yamaji, K., Takemoto, Y., Kirimura, K., Kosaka, S., Matsumoto, H., 2014. Validation of the nodal kinetics code system GALAXY/COSMO-K using the SPERT-III E-core experiments. In: Proceedings of PHYSOR 2014 conference.